

## Sulfur Dioxide at the Venus Cloud Tops, 1978-1986

LARRY W. ESPOSITO,<sup>1</sup> M. COPLEY, R. ECKERT, L. GATES, A. I. F. STEWART,<sup>1</sup> AND H. WORDEN*Laboratory for Atmospheric and Space Physics, University of Colorado, Boulder*

Ultraviolet spectroscopy from the Pioneer Venus Orbiter shows a decline in the cloud top abundance of SO<sub>2</sub> from about 100 ppb to about 10 ppb in the period 1978-1986. A consistent decline in polar haze has occurred over the same period, with the correlation coefficient between these two observables of  $r = 0.8$ . Star calibrations determine the instrument sensitivity to within 10%, which rules out the possibility that this is an instrumental effect. Systematic errors could increase the SO<sub>2</sub> abundance to twice the inferred values in later orbits. Tracking of SO<sub>2</sub> features and power spectral analysis give rotation periods for the longer-lived features of 3.6-5.2 days, consistent with cloud-tracked winds observed at other wavelengths. The behavior of SO<sub>2</sub> and polar haze can be plausibly explained by episodic injection of SO<sub>2</sub> into the cloud top regions, for example, by active volcanism.

## INTRODUCTION

The discovery of sulfur dioxide at the Venus cloud tops in 1978 [Barker, 1979; Conway *et al.*, 1979; Stewart *et al.*, 1979] has profoundly affected our understanding of the Venus clouds and their chemistry [e.g., Winick and Stewart, 1980; Yung and DeMore, 1982]. Additionally, the variability of the SO<sub>2</sub> has led Esposito [1984] to infer active volcanoes on Venus. In this paper we describe the data and model procedures which establish the long- and short-term variability of sulfur dioxide on Venus, as observed by the ultraviolet spectrometer on the Pioneer Venus Orbiter.

## EXPERIMENT DESCRIPTION

The Pioneer Venus Orbiter (PVO) began observations of Venus in 1978 [Colin, 1980]. The orbiter payload includes an ultraviolet spectrometer (UVS), which regularly carries out remote observations of the cloud top region of the atmosphere [Stewart *et al.*, 1979; Stewart, 1980; Esposito *et al.*, 1979; Esposito, 1980]. For the purpose of observing SO<sub>2</sub>, two modes are employed: In the spectral mode the spectrometer grating is advanced as the spacecraft spin carries the instrument optical axis across the planet (the PVO is a spin-stabilized spacecraft). The 4-ms integration period is synchronized with the 4-ms grating dwell period. The full spectral range of 1556 to 3605 Å is covered in two segments of 256 words. Each segment takes 1 s to acquire and is collected on an individual scan of Venus. To minimize the variation of the illumination, emission, and scattering angles during the acquisition of each segment, this mode is used only near PVO periapsis, when the planet's disk subtends an angle much larger than the arc swept out by the optic axis in 1 s. In the wavelength mode the grating position is fixed during each scan: this yields a limb-to-limb profile of planetary brightness. By alternating among several wavelengths in this mode, the UVS observations create a multicolor image of Venus. The basic data for this study of SO<sub>2</sub> are the brightness measured at wavelengths  $\lambda = 207$  nm and  $\lambda = 237$  nm from these two modes of operation, along with the associated observing geometry.

The spatial resolution of the observations depends on the

distance from the spacecraft to the planet and other geometrical factors. Periapsis rose from 150 to 2500 km between 1978 and 1986, and the spatial resolution in spectral mode correspondingly diminished from  $\sim 2$  to  $\sim 75$  km. The resolution of the images also degraded, from  $\sim 400$  to  $\sim 800$  km.

## CALIBRATION

For the spectral analysis that follows, it is essential to know the instrument sensitivity at the wavelengths of observation. For this purpose we have preflight laboratory calibration; in-flight bright star observation, as the PVO was en route to, and in orbit around, Venus; and observations of the planet Venus itself, at locations where the SO<sub>2</sub> absorption is insignificant. These measurements show that the instrument sensitivity has been steadily declining since orbit insertion in 1978, because of aging of the detector tubes. The sensitivity decline is a strong function of wavelength and the rate of decline is also a function of time, with instrument degradation somewhat slowed down after measures were taken to reduce the light dose received by the instrument during regular observations.

It is especially important to know the sensitivity as a function of time, since we will make conclusions in the following discussion about temporal variations of the sulfur dioxide from the spectral observations.

The standard method we have used to track instrument sensitivity is to take spectra of the brightest points in the polar haze [Travis *et al.*, 1979]. The high albedo of these regions of Venus shows that the contribution of any absorber, including SO<sub>2</sub>, is quite small. The brightest spectra from latitude nearest 60°N during a periapse observing season are compared to the model of Kawabata and Hansen [1975] with an additional layer of enhanced polar haze [Kawabata *et al.*, 1980] added to the top of the atmosphere. The optical depth of the polar haze layer is determined by polarimetry at the time of observation. These polar haze optical depths are given by K. Kawabata *et al.* (unpublished data, 1982) and later, by personal communications from L. D. Travis (1987).

This method has the advantage that the calibrating data are collected on the same orbits as the spectral mode data. If the brightness of the polar haze is constant, this directly gives the rate of decline of instrument sensitivity. However, the absolute sensitivity will depend on the accuracy of the photometric model of Kawabata. Nonetheless, even if the brightness is not constant, our analysis will determine the amount of SO<sub>2</sub> at other points on Venus relative to the polar haze. To reduce the scatter, a least squares fit to these data gives the sensitivity

<sup>1</sup>Also at Department of Astrophysical, Planetary, and Atmospheric Sciences, University of Colorado, Boulder.

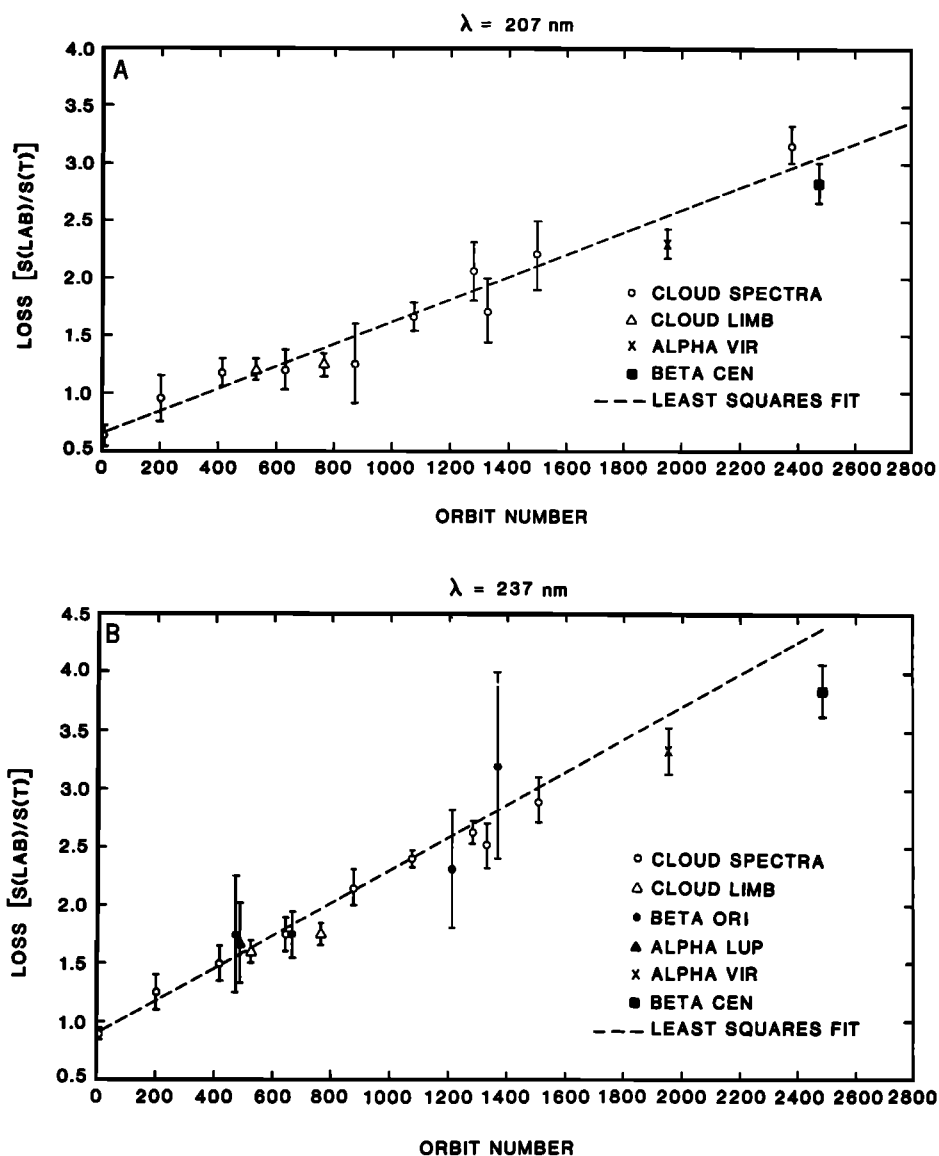


Fig. 1. Sensitivity loss as a function of time. Instrumental sensitivity is compared to preflight laboratory calibration, S(LAB). Cloud spectra: observations of 60°N polar haze, as described in text. Cloud limb: observations of clear Rayleigh scattering above limb. Star calibrations with individual stars noted. Dashed line is least squares fit to calibrating cloud spectra at (a) 207 nm, and (b) 237 nm.

loss as a function of time. These calibrating observations, denoted "cloud spectra," are shown in Figure 1 along with the linear fit.

We have checked this calibration method by observations of stars. The star observations are much more infrequent than our spectral observations. This is because the instrument's field of view (FOV) is normally fixed along a single track in the celestial sphere ( $\sim 30^\circ$ S ecliptical latitude, where only  $\alpha$ Lup and  $\beta$ Ori are available) except for a small wobble. A problem in using the star observations to calibrate the instrument sensitivity is that stars are point sources, unlike the Venus atmosphere. The instrument response for sources which underfill the FOV depends significantly on the source location within the FOV. (That is, the instrument response is not flat across the FOV). We have discovered that in general the normal pointing information supplied by the spacecraft is not accurate enough to determine exactly where a star is within the FOV.

In order to resolve these problems, during 1984 and 1985

the PVO spin axis was precessed on two occasions to observe the bright UV stars Spica ( $\alpha$ Vir) and Hadar ( $\beta$ Cen) and to accurately measure the response variability across the FOV. These results provided reliable instrument sensitivity calibrations and maps of instrument FOV response that allow accurate comparison of discrete and extended sources. In addition, they may be compared to a stellar observation of Spica made during cruise between Earth and Venus: this determines the sensitivity loss over the period 1978–1985.

The stellar calibration results at the two wavelengths used for SO<sub>2</sub> analysis show excellent agreement with the planetary observations of the bright polar haze. At  $\lambda = 207$  nm the decline calculated from Venus is a factor of 4.7. For the star observations the decline is measured as 4.34 (7.7% smaller). At  $\lambda = 237$  nm the Venus observations give a decline of 5.0. The stellar observations give 4.81 (3.8% smaller). Given the accuracy of each of the calibrating methods ( $\lesssim 10\%$ ), we conclude that the instrument sensitivity as a function of time is determined within 10% by two sets of independent measurements

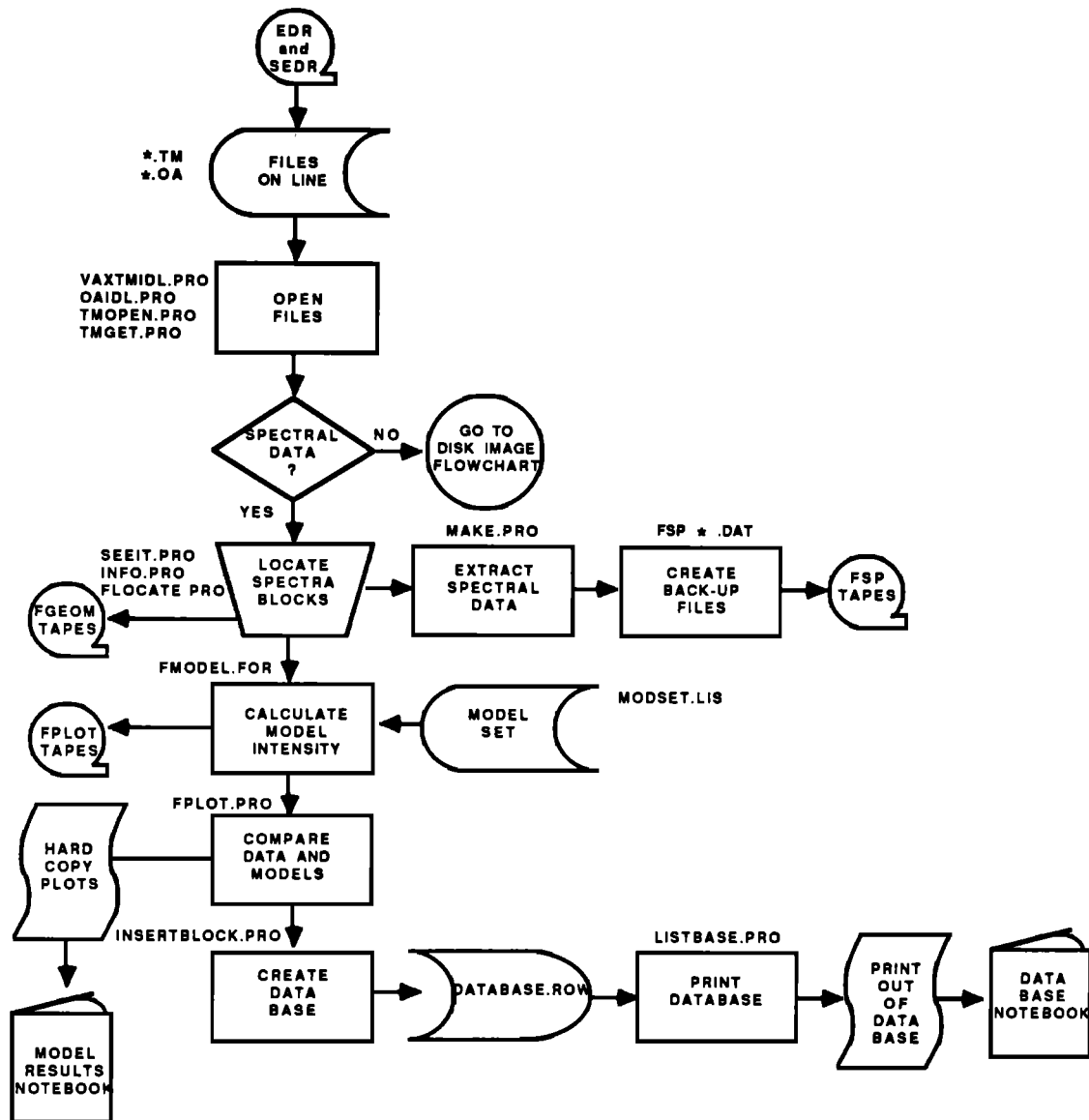


Fig. 2. Flowchart of procedure to determine SO<sub>2</sub> abundance. Processing begins (top) with magnetic tapes and ends (bottom left and right) with archival of results. For multicolor images (middle diamond) processing continues as shown in Figure 3.

over the course of the mission and that the brightness of the polar haze has not changed appreciably over the 8 years of observation. The actual sensitivity used is given by the dashed line in Figure 1.

#### MODEL PROCEDURE

Venus spectral and multicolor data arrive on a regular schedule in the form of magnetic tapes from the Pioneer Venus project at the NASA Ames Research Center. Once the data are in hand at the University of Colorado, the data are handled by a sequence of procedures that result in multicolor rectified images of Venus, SO<sub>2</sub> abundance and scale height for each spectrum, and SO<sub>2</sub> abundance for every picture element in the rectified images. These results are stored in various databases by orbit, latitude, Venus phase, etc. The complete procedure is sketched in the flowchart shown in Figures 2 and 3.

For every observation the brightness at 207 and 237 nm and the instantaneous observing geometry are the input values

to the model procedure. The SO<sub>2</sub> absorption coefficient averaged over the instrument band pass (1.3 nm) differs by a factor of 100 at these two wavelengths [e.g., Thompson *et al.*, 1963]. This difference allow determination of both SO<sub>2</sub> abundance and scale height.

For the spectral data the planetary brightness is compared to a set of 10 brightness models, each calculated using the appropriate observing geometry at two wavelengths. The model parameters are the SO<sub>2</sub> abundance at 40 mbar (essentially the cloud top, see Esposito and Travis [1982]) and the SO<sub>2</sub> scale height (SO<sub>2</sub> is assumed to have an exponential distribution). The model names, SO<sub>2</sub> abundance and scale height are given in Table 1.

For the multicolor images, a subset of seven models (TL, AB2, AA2, A2, B2, D2, E2; see Table 1) are compared to the data. These all have the SO<sub>2</sub> scale height fixed at 2.5 km (the most common value derived from the analyses of the spectral data). The SO<sub>2</sub> abundance has the parameter values 0, 3.125, 6.25, 12.5, 25, 20, and 100 ppb at 40 mbar. Fixing the value of

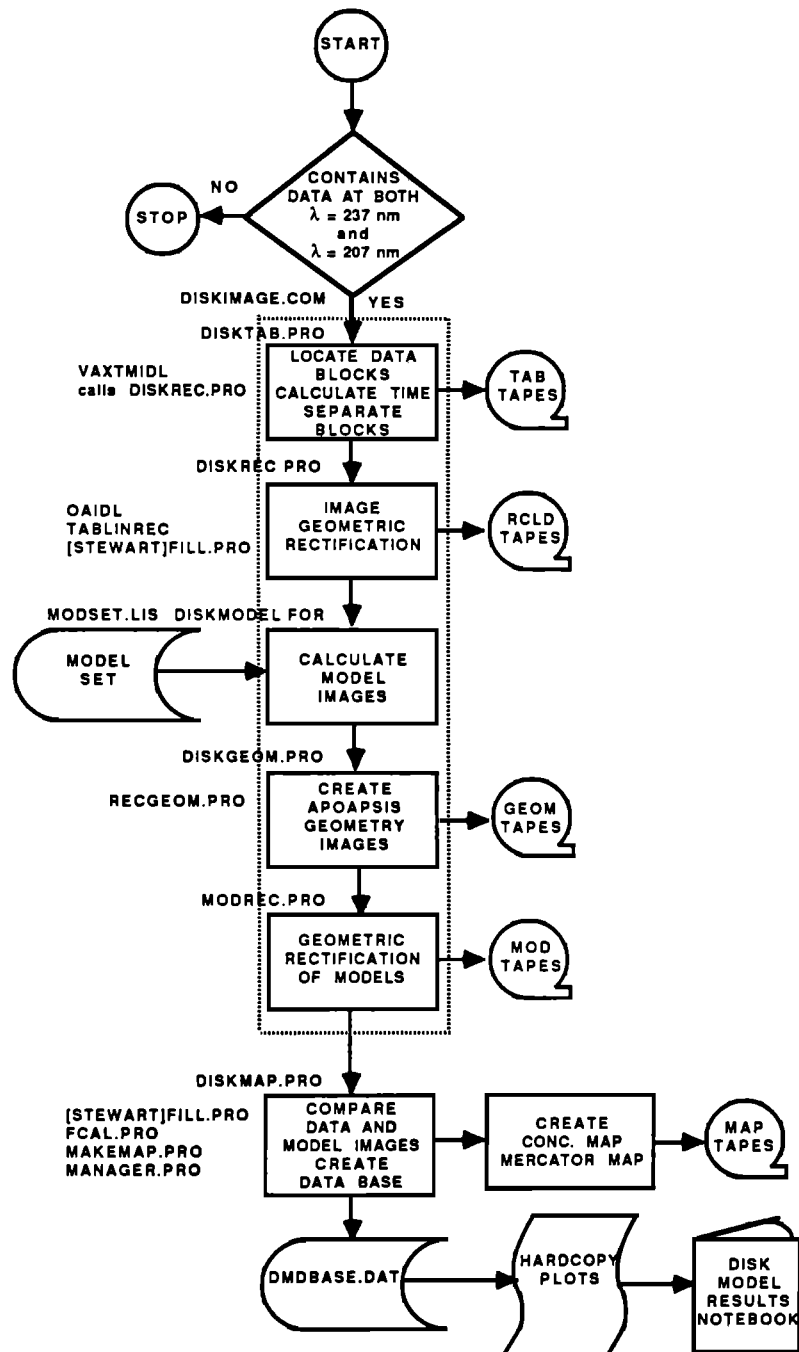


Fig. 3. Flowchart of processing of multicolor images. (Top) Data enter from Figure 2 and procedures end (bottom) with archival of results.

the scale height at 2.5 km substantially reduces the computational effort required in reducing this data set. As can be seen below, the derived SO<sub>2</sub> abundance is in good agreement between the multicolor images and the spectra.

The modeling procedure is similar to that used by *Esposito* [1980]. See Table 2. The reflected brightness is calculated (including multiple scattering, vertical inhomogeneity, and the reported observing geometry) by the method of Markov chains [Esposito, 1979]. The best fit model is the one whose combination of abundance and scale height minimizes the sum of the squares of the difference between model and data at the two wavelengths. If the root-mean-square (rms) difference is greater than 10% of the observed brightness, no model fit is deemed satisfactory. The possible causes of unacceptable fits

are variability of SO<sub>2</sub> in the observed region which is too small to be resolved, random data errors, and the limited number of models to be compared. Of 1545 spectra taken by the UVS in the first 2814 orbits (8 years) a satisfactory fit is found for 1110 (72%). For each of the 157 orbits containing spectra, we average the derived values (which are the SO<sub>2</sub> abundances from the best fit models) to give global means for SO<sub>2</sub> abundance. Global means are also calculated by averaging all the picture elements from a multicolor image that are successfully modeled (i.e., within 10% error). Combining the spectral data with the 195 multicolor images gives a total of 352 orbits, for which we derive individual global mean amounts of SO<sub>2</sub>. These means are plotted in Figure 4.

Figure 4 shows substantial scatter. We believe this scatter is

TABLE 1. Models Used for Spectral Analysis

Model Name	SO <sub>2</sub> Abundance at 40 mbar, (ppb)	Scale Height, km
TL	0.0	
AB2	3.125	2.5
AA2	6.25	2.5
A1	12.5	5.0
A2	12.5	2.5
A3	12.5	1.67
A4	12.5	1.25
B1	25.	5.0
B2	25.	2.5
B3	25.	1.67
B4	25.	1.25
D1	50.	5.0
D2	50.	2.5
D3	50.	1.67
D4	50.	1.25
E1	100.	5.0
E2	100.	2.5
E3	100.	1.67
E4	100.	1.25

real and indicates natural variability of Venus cloud top conditions (similar to “weather” on Earth). The scatter can be reduced by averaging the inferred abundances from the spectra over Pioneer Venus observational seasons (about 100 days). Each of these seasons represents a contiguous period when the planet disk visible to PVO is illuminated at perapse or apoapse observing times. See Figure 5.

RESULTS

Abundance of SO<sub>2</sub>

From Figures 4 and 5 it is obvious that the amount of sulfur dioxide visible at the Venus cloud tops has declined by about 1 order of magnitude since the start of the mission in 1978. This decline has two parts. A rapid decline in the first 400 days of the mission has a characteristic decay time (1/e) of about 200 days. Following this is a slower decline, apparently still in progress, with a decay time of about 2000 days. Given the uncertainties in the instrument calibration, this latter decay rate is marginally consistent with a constant SO<sub>2</sub> abundance and a 10% overestimate in the instrument sensitivity decline. We note that the current abundance of SO<sub>2</sub> is consistent with upper limits set before the Pioneer Venus encounter [e.g., Owen and Sagan, 1972; Cruikshank and Kuiper, 1967].

Correlation With Polar Haze

Travis et al. [1979] have noted several other unusual aspects of the Venus atmosphere at the time of PVO encounter. The cloud images from the PVO Cloud Photopolarimeter (CPP) clearly show bright polar regions. Polarimetry shows that a haze of submicron particles covers the entire planet and is especially evident over the poles. This haze of small particles can account for the bright polar regions. The last major occurrence of bright polar caps in 1959 was also associated with submicron particles at the cloud tops [Dollfus et al., 1979]. It is possible to understand these repeated occurrences in a straightforward way. A simple explanation is as follows.

1. SO<sub>2</sub> is episodically injected above the Venus cloud tops.

2. This SO<sub>2</sub> is rapidly converted to new, small aerosols of H<sub>2</sub>SO<sub>4</sub>, seen as a haze and especially bright polar regions.

3. These aerosols grow and fall out into the main cloud deck, which would give rise to decade-long periods during which neither small aerosols nor SO<sub>2</sub> are seen.

Esposito and Travis [1982] showed that there is a negative correlation between the submicron haze at any given instant and the amount of SO<sub>2</sub>. The natural interpretation of this is a conservation of sulfur atoms as they are exchanged between the gas (SO<sub>2</sub>) and the haze aerosol (H<sub>2</sub>SO<sub>4</sub>). Since the particles are produced from the SO<sub>2</sub> gas, this would naturally explain the observed long-term positive correlation; as the global amount of SO<sub>2</sub> declines, so should the production of haze aerosols. Indeed, K. Kawabata et al. (unpublished data, 1986) show the amount of submicron haze decreased by an order of magnitude over the first 1000 days of the Pioneer Venus mission.

Figure 6 compares our Pioneer Venus UVS data from the first 1600 orbits to seasonally averaged measurements of polar haze optical depth from the Pioneer Venus UVS CPP (K. Kawabata et al., unpublished data, 1986). The correlation is striking: both measures show a strong decline since the beginning of mission, leveling off at more historically typical values after 5 years. The correlation coefficient between these two measures is 0.8. This strongly supports the hypothesis that the polar haze is formed of small, recently created aerosols of H<sub>2</sub>SO<sub>4</sub>.

Cloud Top Rotation Rates

Tracking of cloud features has provided detailed measurements of the wind velocity at cloud top altitudes [e.g., Travis et al., 1979; Rossow et al., 1980; DelGenio and Rossow, 1982]. We have examined the rotation rates of SO<sub>2</sub> features to compare with these with wind measurements.

TABLE 2. Model Atmospheres for Venus SO<sub>2</sub> Abundance

Atmospheric Property	Adopted Characteristics
Clear gas above clouds	5 mbar
Aerosols	total optical depth 20.0 ratio of Rayleigh to aerosol extinction, 0.035 at 3650Å physical characteristics: (1) spherical; (2) refractive index 1.46 at 2650Å;* (3) effective radius 1.05 μ; (4) effective variance 0.07; (5) aerosol single scattering albedo 0.98;
SO <sub>2</sub>	uniformly mixed with gas scale height from Table 1 mixing ratio at 40 mbar from Table 1 maximum mixing ratio: 100 times values from Table 1 uniformly mixed below 150 mbar
Second absorber	altitude 75 mbar optical depth 0.2 single scattering albedo 0.0
Clear gas below clouds	total optical depth 64.0 single scattering albedo given by maximum SO <sub>2</sub> mixing ratio

\*Extrapolated to shorter wavelengths by the method of Hansen and Hovenier [1974].

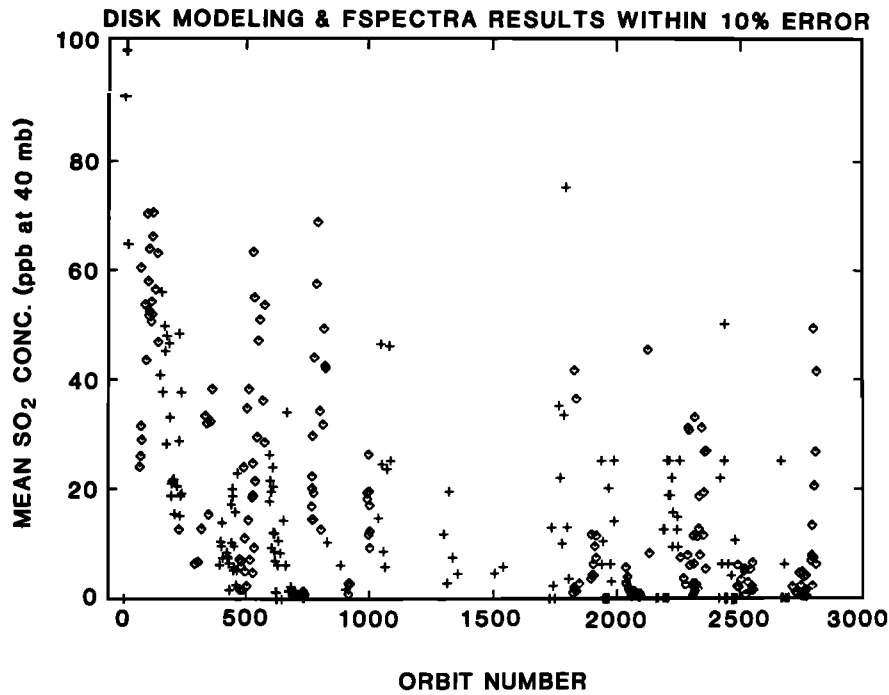


Fig. 4. Mean SO<sub>2</sub> amount for orbits containing spectra (sunlit periapsis, crosses) and multicolor images (sunlit apoapsis, diamonds).

The model procedure (described earlier, see Figure 3), is used to create a map for the portion of the planet which was viewed which represents the SO<sub>2</sub> concentration for the time of observation. A data base of these maps is used in two ways to determine rotation rates from SO<sub>2</sub> abundance variations. The first method involves looking for features which persist for more than 1 Earth day (one Pioneer Venus orbit) using a sequence of maps made for 4 or 5 consecutive days which show a complete rotation of the cloud tops. The second takes the discrete Fourier transform of the sequence of global SO<sub>2</sub> averages in Figure 4.

The procedure for using consecutive orbits is as follows. SO<sub>2</sub> concentration maps are made from 4 or 5 consecutive orbits, and then are converted to mercator projections with Venus latitude as the vertical axis and Venus local solar time (LST) as the horizontal axis. This procedure uses the geometry data obtained from the spacecraft. Each map is discretized into pixels which are 12 min of LST wide and 3° of latitude tall. The map is then 120 pixels wide and 60 pixels tall, where 120 pixels of LST correspond to one complete rotation of the cloud top.

If a SO<sub>2</sub> feature persists for more than 1 day it should be

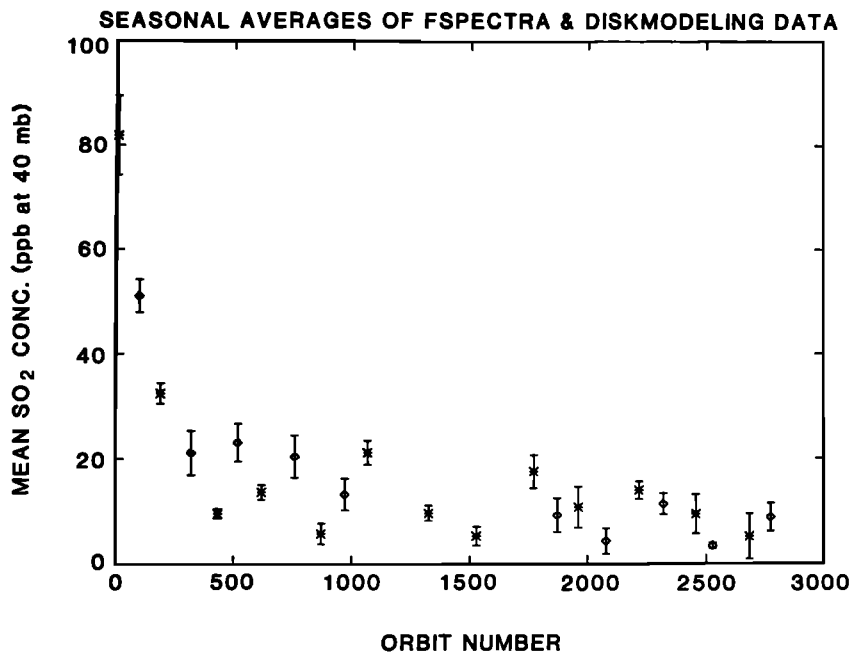


Fig. 5. Mean SO<sub>2</sub> amount averaged over each observing season. Asterisks, sunlit periapsis, diamonds, sunlit apoapsis. Error bars show standard error of the mean.

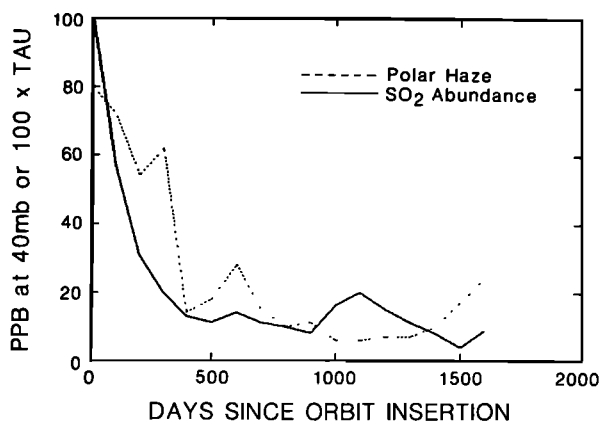


Fig. 6. Intercomparison of derived SO<sub>2</sub> (solid line, this work) and derived polar haze optical depth (dashed line) from PVO Cloud Photopolarimeter (L. D. Travis, personal communication, 1987).

possible to track the feature on successive days as the cloud top rotates. To search for persistent features, overlapping adjacent mercator maps are shifted by integer numbers of pixels along the LST axis, relative to the previous map. Between adjacent maps (e.g. first and second, second and third, third and fourth, but not fourth and first), the overlapping portions of the maps are extracted and a least squares fit determines the correlation of SO<sub>2</sub> abundance in the overlapping portion and the proportionality constant between the measured SO<sub>2</sub> on consecutive days. For each value of shift, i.e., from a shift of 1 pixel to the shift value at which the maps no longer overlap, a correlation coefficient and a proportionality constant are calculated. The total range of periods sampled is 0.5 days to 120 days, which we consider sufficient for observing cloud top motions of SO<sub>2</sub> features. The shift value which gives the highest correlation with a proportionality constant closest to unity determines the rotation period.

For PV orbits 525–528, the derived cloud top rotation period is 4.8 days and the corresponding constant of proportionality was 0.98. This is close to periods calculated by Rossow *et al.* [1980]. However, other consecutive orbit sequences give divergent values from 2 to 6 days and correlation coefficients substantially below 1.0. Thus these results do not seem to be definitive, but do not contradict previous measurements.

For the Fourier transform method, we use the global average SO<sub>2</sub> concentration for each available orbit between orbits 474 and 574, yielding 27 data points. Linear trends in the data are removed by subtracting the mean and first moment, determined by a least squares fit to the data. The same procedure was applied to the maximum value of SO<sub>2</sub> concentration in any latitude bin for each orbit. Those maximum SO<sub>2</sub> data points have the same time distribution as the global SO<sub>2</sub> averages.

Because the data were not obtained every day, we have unequal spacing in the time domain. We note that the actual data spacing is integer numbers of orbits and is not random. Because of a relatively small number of data points and the lack of randomness in the spacing, we chose not to impose equal spacing through interpolation, as this would introduce new and unreliable data points. Instead, we analyze the unweighted, unequally spaced SO<sub>2</sub> abundances.

In determining the best approach to a discrete Fourier transform on unequally spaced data, we considered several

methods, finally choosing the relatively simple procedure proposed by Deeming [1975]. In choosing this method, however, we necessarily lose the possibility for the somewhat rigorous error analysis available in the method of Ponman [1981]. Ponman's method, however, works better for data which has no regularity in the time spacing, while our data has inherent regularity due to different factors, among which is the weekly scheduling of spacecraft commands for the Pioneer Venus Orbiter. Ponman [1981] deals with the general case of data which is irregularly sampled, weighted, and integrated over time (possibly different for each data point).

Deeming [1975], however, assumes instantaneous observations, which is better suited to our data: although the image of the planet is taken over  $\sim 2$  hours, a rectification procedure (part of the normal processing in Figure 2) is applied to each image to create another image corresponding one point in time, giving an "instantaneous" observation.

Deeming [1975] defines a discrete Fourier transform  $F(\nu)$  of  $f[t(k)]$ , for arbitrary time spacing  $t(k)$  of  $N$  data points, as follows:

$$F(\nu) = \sum_{k=1}^N f[t(k)] \exp [2\pi i \nu t(k)]$$

The spectral window

$$W(\nu) = \sum_{k=1}^N \exp [2\pi i \nu t(k)]$$

also known as a "data window," contains the "pathology" of the data spacing, including aliasing and related effects.  $F(\nu)$  represents the convolution of the "true" Fourier transform of the function which the data represent with the spectral window.

The problem of aliased peaks in the discrete Fourier transform places a constraint on the maximum frequency for which reliable information can be calculated. Aliasing occurs at frequencies above a Nyquist frequency which is calculated from the data spacing. For equally spaced data there is only one Nyquist frequency:  $\nu_0 = 1/2\Delta t$ , where  $\Delta t$  is the constant time spacing. The results of aliasing are a Fourier transform at  $\nu > \nu_0$  which has a significant contribution from the transform at  $\nu - \nu_0$ . For equal spacing, this aliasing is complete, and frequencies above the Nyquist frequency are indistinguishable from their corresponding frequencies below the Nyquist frequency. The data spacing of the available SO<sub>2</sub> concentrations, although unequal, is in integer multiples of a smallest unit spacing (1 orbit = 1 day). This leads to the possibility of several Nyquist frequencies, with the maximum as the Nyquist frequency for equal spacing,  $1/2$  orbits<sup>-1</sup>. This is then the highest frequency calculated in the discrete Fourier transform.

Normalization of the spectral window represents another procedural difficulty. Ideally, the spectral window should be square integrable to unity. However, since this is only possible in an approximate sense, it is easier and more useful to "normalize" the spectral window by setting  $W(0) = 1$ . This is done simply by dividing the original function  $W(\nu)$  by the number of data points  $N$  (over which  $W(\nu)$  is summed), as Deeming proposes. Then, for equal time spacing, the spectral window is unity at integer values of  $\nu$  and zero elsewhere. For unequal spacing,  $W(\nu)^2$  may be large for nonintegral values of  $\nu$ , but less than unity. These secondary peaks in the spectral window produce artifact peaks in the discrete Fourier transform. This is because the discrete Fourier transform represents the convo-

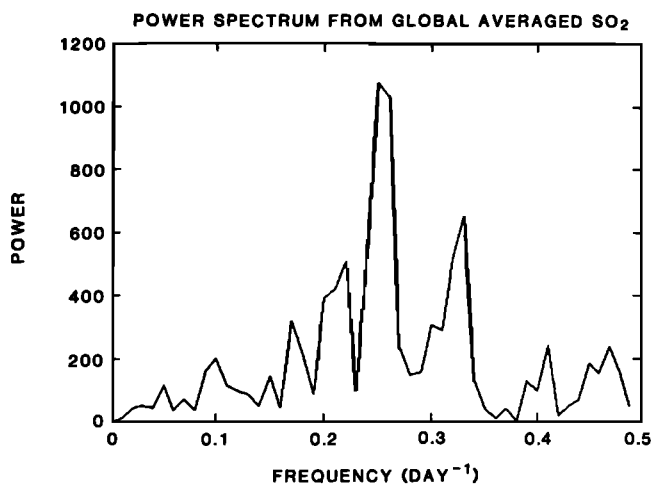


Fig. 7. Power spectrum of mean SO<sub>2</sub> for orbits containing spectra between 474 and 574. Peak at  $\nu = 0.25 \pm 0.03$ .

lution of the true Fourier transform with the spectral window and, if the spectral window has peaks which are artifacts of the data spacing, the effects of these peaks will then be present in the convolution.

The Fourier transform of the data is normalized differently from the spectral window, so that the transform is symmetric and approximately obeys Parseval's theorem; that is, average power is nearly equal in the time and frequency domains. The FORTRAN code used is very close to that proposed by Deeming, with minor adjustment for the different normalization (we divide the power by  $N$  instead of  $N^2$ ).

The two calculated power spectra are shown in Figures 7 and 8. The power of the spectral window for the time spacing of both data sets is shown in Figure 9. The main peak in both frequency power spectra is at  $0.25 \pm .03$  (Earth days)<sup>-1</sup>, giving a rotation period of  $4.0 \pm 0.5$  Earth days for the cloud top. In the spectral window the first artifact peak at  $\nu = 0.14$  represents a weekly periodicity (scheduling of spacecraft commands is on a weekly basis). The second artifact peak at  $\nu = 0.43$  represents a mean sampling rate of 3 orbits per week. This arises because an average of three out of every seven orbits have the spectral or multicolor data which we can use to calculate SO<sub>2</sub> concentration. The primary peak in the spectral window, at  $\nu = 0$ , has the value 1.0, as expected.

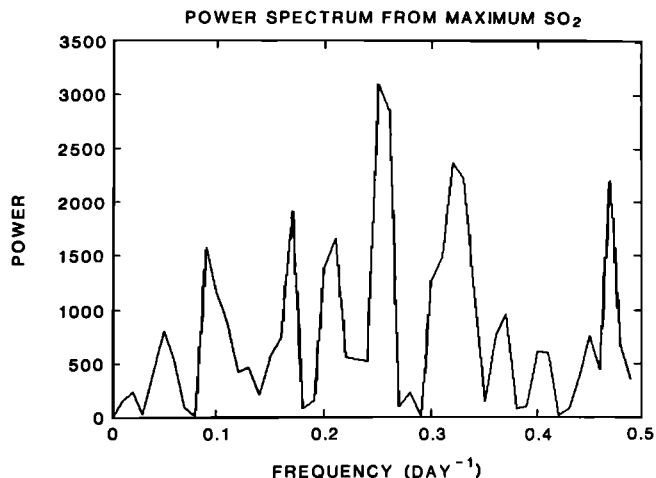


Fig. 8. Power spectrum of maximum concentration averaged over 10° latitude bins from orbits 474 to 574.

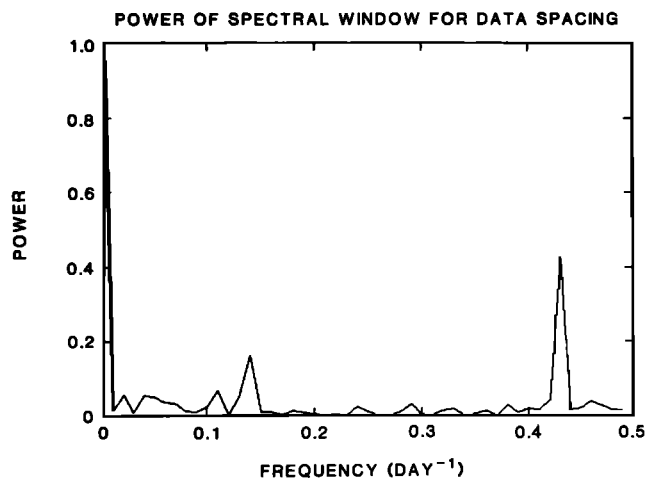


Fig. 9. Power of spectral window for actual time spacing of orbits containing spectra 474–574.

The same analysis was performed on SO<sub>2</sub> concentrations derived from modeling  $F$  spectra. This data set of all available SO<sub>2</sub> concentrations between orbits 2160 and 2255 also had the mean and first moment removed. The result of the discrete Fourier transform was a power spectrum with a peak of 0.22, corresponding to a period of  $\sim 4.5$  days. The spectral window for this data set is similar to the earlier spectral window, with a large secondary peak at 0.43 ( $3/7$  day<sup>-1</sup>).

These analyses show rotation rates for SO<sub>2</sub> features comparable to Venus mean cloud top rotation ( $\sim 4.8$  days) and rotation of the dark "Y" feature (4–5 days), as determined by Rossow *et al.*, 1980.

## DISCUSSION

### Sources of Error and Uncertainty in SO<sub>2</sub> Abundance

The data analyzed here represent the longest uniform spectroscopic data set for the planet Venus. Identical Venus observations have been made on a weekly basis for more than 8 years, and those observations have been reduced and analyzed using a single established protocol. This analysis, although optimized to measure SO<sub>2</sub> abundance, has a number of imperfections, which we now discuss.

The total decline of instrument sensitivity over the length of the mission is now known within 10%, because of careful star calibrations. However, we have modeled this as a purely linear decline. Some evidence shows that the rate of decline is less in recent years. This means that the abundance of SO<sub>2</sub> in the last 1000 days may be underestimated by up to 50%. Likewise, any other deviations from linear behavior have been interpreted as SO<sub>2</sub> variability. This means that short-term trends should not be overinterpreted.

A second characteristic of the analysis is the use of a simple two-parameter model (SO<sub>2</sub> abundance at 40 mbar and scale height at 40 mbar). Model results are only calculated for discrete pairs of these parameters. Venus is certainly more complicated than this! For example, the assumption of a simple exponential distribution with a constant scale height is certainly wrong. As the mixing ratio of SO<sub>2</sub> declines, the photochemical lifetime of SO<sub>2</sub> increases until diffusion dominates. Eventually, a constant mixing ratio is established in the stratosphere, causing the SO<sub>2</sub> scale height to increase with altitude. Such an effect would be evident from observations at different

zenith angles. However, our abundance determination show no strong dependence on zenith angle [see *Esposito*, 1984]. Thus while ignoring this effect provides a source of error in our determinations, we have insufficient information to correct for it. We guard against some problems by not using data which do not lie within 10% rms of one of the model spectra.

The models were originally tuned to match real data in the first 200 orbits. After this, the model set was fixed. As Venus has changed over the years, the model set has not. This has the advantage of uniformity, but a disadvantage in that the later orbits are not as well spanned by the model set.

The models include a number of assumptions about the Venus atmosphere. For example, the amount of the second, unknown UV absorber is assumed constant and to have a flat absorption spectrum over the wavelengths of interest (see Table 2). The submicron haze varies only in the polar region model in a slow way that accounts for the broad long-term trends measured by the CPP. As the SO<sub>2</sub> abundance declines, these other scattering components have become more important, thus decreasing the reliability of our SO<sub>2</sub> abundance determinations.

The intrinsic variability of SO<sub>2</sub> also provides some limit on the accuracy of determining its mean global abundance. Our results show that the mean amount of SO<sub>2</sub> visible on consecutive days can vary by a factor of 4. Horizontal variability provides another limitation. Spacecraft images clearly show structure in the absorption features smaller than our best image resolution (about 400 km square), and occasionally smaller than our spectral mode resolution (as large as 80 km). This unresolved structure can cause none of the models to fit the observation or an underestimate of the mean SO<sub>2</sub> abundance.

The general agreement of the image and spectral abundance determinations (see Figure 5) shows that horizontal structures with scales resolved by the spectral mode observations but not by the imaging mode do not contribute to significant errors in our derived abundances. However, scale lengths shorter than this may give rise to incorrect abundances.

Altogether, however, we believe that observations over a season (see Table 3) approximate the actual global means and that the data quality does not justify a model with substantially more parameters or allowance for unresolved horizontal variability. In the interests of uniformity we have not tinkered with the model set as a function of time. Because of these considerations the systematic errors in the later determinations are probably larger than those in the first 400 orbits. A number of these systematic errors go in the same direction, so that SO<sub>2</sub> abundance may be underestimated by 50–100% in the last 1000 orbits. In the worst case this could be consistent with no significant decline in SO<sub>2</sub> abundance after orbit 1500.

#### Active Venus Volcanoes

*Esposito* [1984] has interpreted the observed SO<sub>2</sub> injection and resulting haze formation as due to episodic volcanism. Radar studies by the Pioneer Venus Orbiter [*Masursky et al.*, 1980] have detected topographic features on Venus that resemble terrestrial volcanic landforms. *Prinn* [1985] argues that the observed amount of SO<sub>2</sub> in the lower atmosphere is out of equilibrium with the surface composition measured by the latest Venera landers [*Moroz*, 1983]. This current imbalance requires a geologically recent source of sulfur compounds at the surface.

It is well known that major volcanic eruptions give rise to a haze layer of submicron particles in the Earth's atmosphere. The mass of aerosols in the Earth's stratosphere after the eruptions of El Chichón in 1982 approached 10<sup>13</sup>g [*Thomas et al.*, 1983]. Vertical optical depths measured in the Earth's polar regions exceeded 0.1. The total mass of the Venus polar haze inferred [*Kawabata et al.*, 1980] is 2 × 10<sup>14</sup>g; the optical depth of the Venus polar haze exceeds 1.0. Thus the amount of aerosols injected into the Venus middle atmosphere is greater by at least an order of magnitude than that associated with the most recent volcanic episodes on Earth.

*Phillips and Malin* [1983] have suggested volcanic activity may be more vigorous on Venus than on Earth because of the lack of organized plate tectonics on Venus. The more vigorous volcanic activity on Venus might be due to larger volcanoes, a greater number of volcanoes, or more frequent eruptions. The last two of these possibilities could account for a higher frequency of SO<sub>2</sub> injections into the visible Venus atmosphere. It should be noted that the injection of SO<sub>2</sub> to cloud heights requires a substantial explosive eruption. Theoretical expectations of lower volatile inventory and the higher Venus surface temperature would make such explosions less likely on Venus.

Recently, *Taylor and Cloutier* [1986] have criticized the interpretation of Pioneer Venus observations as evidence for lighting and the more general idea of active volcanoes on Venus. Their arguments against volcanoes repeat some of the cautions enumerated by *Esposito* [1984]. The case for volcanoes erupting now is clearly still open. However, the volcano hypothesis explains the major aspects of the SO<sub>2</sub> behavior, the polar haze decline, and the recurrence of bright Venus polar caps. This hypothesis fits well with electromagnetic, geochemical, topographic, and tectonic evidence showing geologically recent volcanic activity [see *Esposito*, 1984].

TABLE 3. Seasonal Mean SO<sub>2</sub> Abundance

	Mean PVO orbit	Date	Derived SO <sub>2</sub> Abundance at 40 mbar, ppb
Sunlit periapsis seasons			
1	8	Dec. 12, 1978	82
2	191	June 13, 1979	32
3	433	Feb. 11, 1980	10
4	619	Aug. 15, 1980	14
5	871	April 25, 1981	6
6	1067	Nov. 7, 1981	21
7	1326	July 24, 1982	10
8	1527	Feb. 10, 1983	5
9	1771	Oct. 12, 1983	18
10	1961	April 19, 1984	11
11	2216	Dec. 29, 1984	14
12	2455	Aug. 25, 1985	9
13	2681	April 8, 1986	5
Sunlight apoapsis seasons			
1	100	March 14, 1979	51
2	320	Oct. 21, 1979	21
3	519	May 7, 1980	23
4	759	Jan. 2, 1981	20
5	971	Aug. 3, 1981	13
9	1871	Jan. 20, 1984	9
10	2077	Aug. 12, 1984	4
11	2318	April 10, 1985	11
12	2527	Nov. 5, 1985	3
13	2771	July 7, 1986	9

However, we will not know for certain that volcanoes are erupting until we have a direct sighting or observe before-and-after topography. The best opportunity for this is from the radar imaging on the Magellan mission, to be launched to Venus later in this decade.

#### CONCLUSIONS

Pioneer Venus spectroscopy of the Venus cloud tops shows a decline by about a factor of 10 in the amount of SO<sub>2</sub> since 1978. A consistent decline is also seen in the amount of polar haze, which was also unusually abundant in 1978. Star calibrations determine the instrument sensitivity well enough to rule out the decline as an instrumental effect. Systematic errors are probably larger in the later orbits and may be as large as 50–100% for the SO<sub>2</sub> abundance. A plausible explanation for the observed behavior is injection of SO<sub>2</sub> into the Venus middle atmosphere by a volcanic explosion [Esposito, 1984].

The assumed injection can account for the current geochemical imbalance between the surface and atmosphere, noted by Prinn [1985] and also the failure of steady state photochemical models to match both the small-scale height of SO<sub>2</sub> and the upper limits on O<sub>2</sub>. Since SO<sub>2</sub> is the major precursor of the Venus clouds and is an important absorber of solar radiation, steady state models of the chemistry and dynamics of the cloud top region must be used cautiously. The abundances of other chemically active constituents, such as Cl<sub>2</sub>, CO, and polymorphic sulfur, must also experience coupled episodic variations.

*Acknowledgments.* Larry Travis supplied the information on polar haze optical depths. We have had helpful discussions with Y. L. Yung and H. Masursky. The Pioneer Project Office allowed us to turn the spacecraft to observe stars. This work has been supported by the Pioneer Venus Project Office and the NASA Planetary Atmospheres Program (NAGW-389).

#### REFERENCES

- Barker, E. S., Detection of SO<sub>2</sub> in the UV spectrum of Venus, *Geophys. Res. Lett.*, **6**, 117–120, 1979.
- Colin, L., The Pioneer Venus program, *J. Geophys. Res.*, **85**, 7575–7598, 1980.
- Conway, R. R., R. P. McCoy, and C. A. Barth, IUE detection of sulfur dioxide in the atmosphere of Venus, *Geophys. Res. Lett.*, **6**, 629–631, 1979.
- Cruikshank, D. P., and G. P. Kuiper, An upper limit for the abundance of SO<sub>2</sub> in the Venus atmosphere, *Commun. Lunar Planet. Lab.*, **6**, 196, 1967.
- Deeming, T. J., Fourier analysis with unequally-spaced data, *Astrophys. Space Sci.*, **36**, 137–158, 1975.
- DelGenio, A. D., and W. B. Rossow, Temporal variability of ultraviolet cloud features in the Venus stratosphere, *Icarus*, **51**, 391–415, 1982.
- Dollfus, A., M. Aurière, and R. Santer, Wavelength dependence of polarization, XXXVII, Regional observations of Venus, *Astron. J.*, **84**, 1419–1436, 1979.
- Esposito, L. W., An adding algorithm for the Markov chain formalism for radiative transfer, *Astrophys. J.*, **233**, 661–663, 1979.
- Esposito, L. W., Ultraviolet contrasts and the absorbers near the Venus cloud tops, *J. Geophys. Res.*, **85**, 8151–8157, 1980.
- Esposito, L. W., Sulfur dioxide: Episodic injection shows evidence for active Venus volcanism, *Science*, **223**, 1072–1074, 1984.
- Esposito, L. W., and L. D. Travis, Polarization studies of the Venus UV contrasts: Cloud height and haze variability, *Icarus*, **51**, 374–390, 1982.
- Esposito, L. W., J. R. Winick, and A. I. Stewart, Sulfur dioxide in the Venus atmosphere: Distribution and implications, *Geophys. Res. Lett.*, **6**, 601–604, 1979.
- Hansen, J. E., and J. W. Hovenier, Interpretation of the polarization of Venus, *J. Atmos. Sci.*, **31**, 1137–1160, 1974.
- Kawabata, K., and J. E. Hansen, Interpretation of the variation of polarization over the disk of Venus, *J. Atmos. Sci.*, **32**, 1133–1139, 1975.
- Kawabata, K., D. Coffeen, J. Hansen, W. Lane, M. Sato, and L. Travis, Cloud and haze properties from Pioneer Venus polarimetry, *J. Geophys. Res.*, **85**, 8129–8140, 1980.
- Moroz, V. I., Summary of preliminary results of the Venera 13 and Venera 14 missions, in *Venus* edited by D. M. Hunten, pp. 45–68, University of Arizona Press, Tucson, 1983.
- Masursky, H., E. Eltason, P. G. Ford, G. E. McGill, G. H. Pettengill, G. C. Schaber, and G. Schubert, Pioneer Venus radar results: Geology from images and altimetry, *J. Geophys. Res.*, **85**, 8232–8260, 1980.
- Owen, T., and C. Sagan, Minor constituents in planetary atmospheres: Ultraviolet spectroscopy from the Orbiting Astronomical Observatory, *Icarus*, **16**, 557–568, 1972.
- Phillips, R. J., and M. C. Malin, The interior of Venus and tectonic implications, in *Venus*, edited by D. M. Hunten, pp. 159–214, University of Arizona Press, Tucson, 1983.
- Ponman, T., The analysis of periodicities in irregularly sampled data, *Mon. Not. R. Astron. Soc.*, **196**, 583–596, 1981.
- Prinn, R. G., The photochemistry of the atmosphere of Venus, in *Photochemistry of Atmospheres*, edited by J. Levine, Academic, Orlando, Fla., 1985.
- Rossow, W. B., A. D. DelGenio, S. S. Limaye, L. D. Travis, and P. H. Stone, Cloud morphology and motions from Pioneer Venus images, *J. Geophys. Res.*, **85**, 8107–9128, 1980.
- Stewart, A. I., Design and operation of the Pioneer Venus Orbiter ultraviolet spectrometer, *IEEE Trans. Geosci. Remote Sens.*, **GE-18**, 65–70, 1980.
- Stewart, A. I., D. E. Anderson, L. W. Esposito, and C. A. Barth, UV spectroscopy of Venus: Initial results from the Pioneer Venus Orbiter, *Science*, **203**, 777–779, 1979.
- Taylor, H. A., and P. A. Cloutier, Venus: Dead or Alive? *Science*, **234**, 1087–1093, 1986.
- Thomas, G. E., B. M. Jakosky, R. A. West, and R. W. Sanders, Satellite limb-scanning thermal infrared observations of the El Chichón stratospheric aerosol: First results, *Geophys. Res. Lett.*, **10**, 997–1000, 1983.
- Thompson, B. A., P. Hartek, and R. V. Reeves, Jr., Ultraviolet absorption coefficients of CO<sub>2</sub>, CO, O<sub>2</sub>, H<sub>2</sub>O, N<sub>2</sub>O, NH<sub>3</sub>, NO, SO<sub>2</sub>, and CH<sub>4</sub> between 1850 and 4000 Å, *J. Geophys. Res.*, **68**, 6431–6436, 1963.
- Travis, L. D., D. L. Coffeen, J. E. Hansen, K. Kawabata, A. Lacin, W. A. Lane, S. S. Limaye, and P. H. Stone, Orbiter cloud photopolarimeter investigation, *Science*, **203**, 781–785, 1979.
- Winick, J. R., and A. I. F. Stewart, Photochemistry of SO<sub>2</sub> in Venus' upper cloud layers, *J. Geophys. Res.*, **85**, 7849–7860, 1980.
- Yung, Y. L., and W. B. DeMore, Photochemistry of the atmosphere of Venus: Implications for atmospheric evolution, *Icarus*, **51**, 199–247, 1982.
- M. Copley, R. Eckert, L. W. Esposito, L. Gates, A. I. F. Stewart, and H. Worden, Laboratory for Atmospheric and Space Physics, Campus Box 392, University of Colorado, Boulder, CO 80309.

(Received October 1, 1987;  
revised January 22, 1988;  
accepted January 22, 1988.)